A theoretical and experimental analysis of higher-order Laue zone line splittings caused by a dislocation in an icosahedral quasi-crystal

1992 J. Phys.: Condens. Matter 4 9247

(http://iopscience.iop.org/0953-8984/4/47/006)

J. Phys.: Condens. Matter 4 (1992) 9247–9254. Printed in the UK

A theoretical and experimental analysis of higher-order Laue zone line splittings caused by a dislocation in an icosahedral quasi-crystal

Jianglin Feng, Mingxing Dai, Renhui Wang and Huamin Zou

Department of Physics, Wuhan University, 430072 Wuhan, People's Republic of China and Beijing Laboratory of Electron Microscopy, Academia Sinica, PO Box 2724, 100080 Beijing, People's Republic of China

Received 26 February 1992, in final form 3 August 1992

Abstract. Twelve convergent-beam electron diffraction patterns from an icosahedral phase specimen containing a dislocation along 12 different zone axes, which are equivalent according to icosahedral symmetry, have been photographed and simulated using dynamical theory. The splitting behaviours of higher-order Laue zone lines in these patterns have been analysed in detail. Some deviations between the experimental and theoretical patterns can be explained because the incident probe becomes too close to the dislocation core.

1. Introduction

As it is similar to the case of crystals, the induction of dislocations in the quasi-crystalline icosahedral phase can also result in the splitting and shifting of higher-order Laue zone (HOLZ) lines, as was observed by Wang and Dai [1]. Zhang *et al* [2] found that the Burgers vector of a dislocation in an icosahedral Al–Cu–Fe alloy is parallel to a twofold axis using the diffraction contrast method. On the other hand, Cheng and Wang [3] proposed the dynamical theory for quasi-crystals. On the basis of this theory, Feng *et al* [4] studied the influence of some experimental parameters on the behaviours of the HOLZ line splitting. They found that, the greater the value of $\vec{g} \cdot \vec{b}$ for a HOLZ reflection, the more severely the HOLZ line splits; the degree of splitting increases as the distance between electron probe and dislocation core decreases; when the distance is too small, the intensity of the two main split fringes from a HOLZ line will reverse; the separation between the two split fringes will become larger as the foil thickness decreases. Since the investigation of HOLZ line splitting behaviours may throw light on the strain field of a dislocation in quasi-crystals, we studied the splitting of HOLZ lines by means of simulations as well as by means of experiments on 12 convergent-beam electron diffraction (CBED) patterns taken from the zone axes which are different but equivalent to each other according to icosahedral symmetry. In this paper, we report the results of our experiments and the dynamical simulations.

0953-8984/92/479247+08$07.50

2. Experimental details

$Al_{65}Cu_{20}Fe_{15}$ alloy was prepared by melting the high-purity elements in an arc furnace under an Ar atmosphere. After slow cooling to room temperature the ingot was cut into slices. The specimens for transmission electron microscopy (TEM) were prepared by mechanical thinning and argon ion milling. TEM experiments were carried out on a Philips EM-420 electron microscope at an accelerating voltage of 100 kV. The diffraction contrast image of a dislocation was observed at room temperature with a double-tilting stage. HOLZ line patterns were photographed in the nanoprobe mode with an incident electron probe about 4 nm in diameter using a liquid-nitrogen-cooled double-tilting stage.

3. Dynamical simulation

The computer program was established on the basis of wave mechanical formulation of the many-beam dynamical theory developed by Jones *et al* [5], using the scattering matrix method [6]. The theory for crystals was extended to the case of quasi-crystals recently by Cheng and Wang [3] as follows. Firstly, for the quasi-crystalline icosahedral phase with six degrees of freedom the term $\boldsymbol{g} \cdot \boldsymbol{R}$ is replaced by the inner product in six-dimensional (6D) space:

$$\tilde{\boldsymbol{g}} \cdot \tilde{\boldsymbol{R}} = \boldsymbol{g}^{\parallel} \cdot \boldsymbol{R}^{\parallel} + \boldsymbol{g}^{\perp} \cdot \boldsymbol{R}^{\perp} \tag{1}$$

where the term $\boldsymbol{g}^{\perp} \cdot \boldsymbol{R}^{\perp}$ represents the effect of the phason and $\tilde{\boldsymbol{g}} = \boldsymbol{g}^{\parallel} + \boldsymbol{g}^{\perp}$, $\tilde{\boldsymbol{R}} = \boldsymbol{R}^{\parallel} + \boldsymbol{R}^{\perp}$ with $\boldsymbol{g}^{\parallel}$ and $\boldsymbol{R}^{\parallel}$ being the components in physical space and $\boldsymbol{g}^{\perp}$ and $\boldsymbol{R}^{\perp}$ the components in complementary space of the 6D reciprocal vector $\tilde{\boldsymbol{g}}$ and displacement vector $\tilde{\boldsymbol{R}}$, respectively. The components of the displacement vector $\tilde{\boldsymbol{R}}$ in 6D space can be expressed as

$$R_a = (1/2\pi)\{b_a\phi + \eta_a \sin(2\phi)/4(1-\nu) + \epsilon_a[(1-2\nu)\ln|r|/2(1-\nu) + \cos(2\phi)/4(1-\nu)]\} \qquad (a = 1,2,\ldots,6) \tag{2}$$

where r, ν and ϕ have the same meanings as in crystals [6]; b_a, η_a and ϵ_a are the components of the vectors $\tilde{\boldsymbol{b}}$, $\tilde{\boldsymbol{b}}_e$ and $\tilde{\boldsymbol{\epsilon}}$ in 6D space; $\tilde{\boldsymbol{b}}$, $\tilde{\boldsymbol{b}}_e$ and $\tilde{\boldsymbol{\epsilon}}$ correspond to $\boldsymbol{b}$, $\boldsymbol{b}_e$ and $\boldsymbol{b} \times \boldsymbol{u}$ in crystals ($\boldsymbol{b}$ is the Burgers vector, $\boldsymbol{b}_e$ is the edge component of $\boldsymbol{b}$ and $\boldsymbol{u}$ is the unit vector of the direction of the dislocation line). Secondly, the extinction distance ξ_g of the icosahedral phase is calculated from

$$1/\xi_g = S(\boldsymbol{g}^{\parallel})/\pi V K \tag{3}$$

with K being the magnitude of the wavevector $\boldsymbol{k}$ and $S(\boldsymbol{g}^{\parallel})/V$ the scattering amplitude per unit volume. According to Elser [7] and Zhao *et al* [8], $S(\boldsymbol{g}^{\parallel})$ is expressed as

$$S(\boldsymbol{g}^{\parallel}) = \sum_{1 \leqslant i < j < k \leqslant 6} S_1(i,j,k) S_2(i,j,k) \tag{4}$$

where $S_1(i,j,k)$ represents the phase relationship between all the rhombohedra constructed by $\{e^i, e^j, e^k\}$; $S_2(i,j,k)$ represents the structure factor of this type of rhombohedron. The values $S_2(i,j,k)$ depend on the atomic decoration in rhombohedra. The simple quasi-lattice model [7] was used in our calculations.

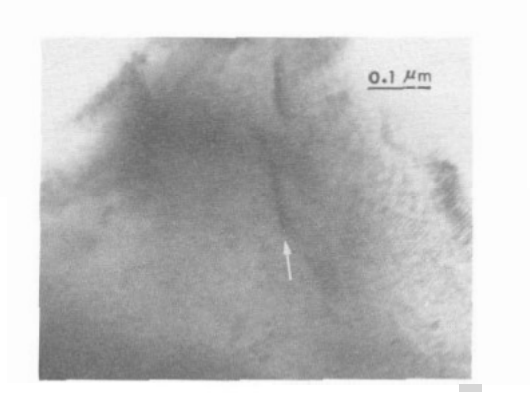

Figure 1. Diffraction contrast image of a dislocation (arrowed) in the icosahedral phase of $Al_{65}Cu_{20}Fe_{15}$ (bright field).

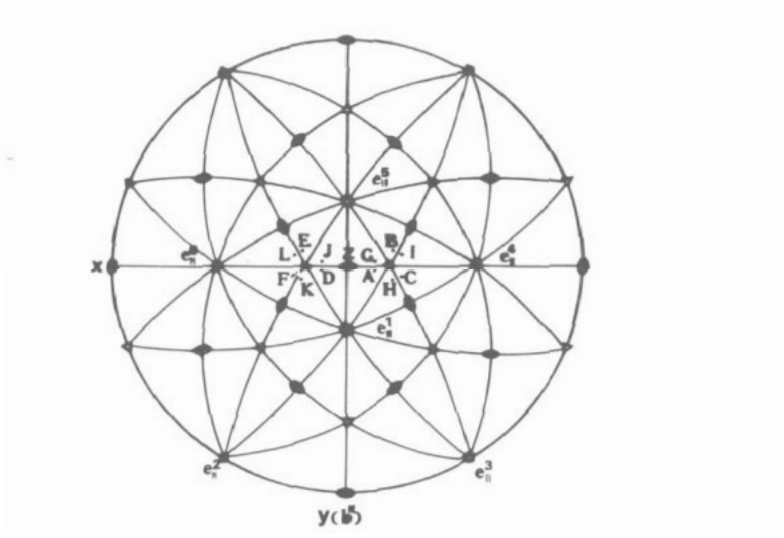

Figure 2. Twelve equivalent orientations in the icosahedral phase corresponding to 12 zone axes A, B, ..., L in the experiments, where b'' is the Burgers vector in physical space and x, y, z are the coordinate axes.

4. Results

Figure 1 shows the bright-field diffraction contrast image of a line defect (arrowed).

The 12 equivalent orientations around two threefold axes according to icosahedral symmetry are shown in figure 2. The indices of four main HOLZ reflections in each zone axis pattern are given in table 1. Owing to the icosahedral symmetry, reflections A3 and G3, B3 and I3, C3 and H3, J3 and D3, E3 and L3, F3 and K3, respectively, are identical reflections, while D2 and G2, J2 and A2, B1 and K1, E1 and H1, etc, are $\pm$ reflections.

Figure 3 shows the 12 HOLZ line patterns along the 12 equivalent zone axes, for which the electron beam was focused near the dislocation. For the perfect icosahedral

Table 1. The indices, the values of $\vec{g} \cdot \vec{b}$ and the signs of δ of the four main HOLZ lines for each pattern in figure 3 and figure 4, the separations d between the electron probe and the dislocation core and the intensity ratios r for each pattern in figure 3, where N indicates the fact that the corresponding HOLZ line is not in the pattern or splits unclearly, and B indicates that it is broadened.

Zone axes	d		Indices of HOLZ lines						$\vec{g} \cdot \vec{b}$	r	sign(δ)
A	15	A1	4	8	2	−4	−2	6	2.5	0.5	−
		A2	−4	−8	−6	2	4	−2	−3.5	0.8	+
		A3	2	4	−4	−6	2	8	0.0	0.0	
		A4	−2	−4	2	4	0	−6	−0.5	0.2	+
B	−15	B1	−4	−6	−8	−2	4	2	−3.5	0.6	−
		B2	2	2	8	4	−4	−6	2.5	0.2	+
		B3	−6	−8	−4	2	2	−4	−3.0	0.3	−
		B4	4	6	4	0	−2	2	2.5	0.4	+
C	−12	C1	−2	−2	6	4	−4	−8	1.0	B	
		C2	4	6	−2	−4	2	8	1.0	0.4	+
		C3	2	4	8	2	−6	−4	3.0	1.0	
		C4	0	−2	−6	−2	4	4	−2.0	1.0	
D	−10	D1	4	2	8	6	−2	−4	2.5	0.9	+
		D2	−4	−6	−8	−2	4	2	−3.5	1.0	
		D3	2	−4	4	8	2	−6	0.0	B	
		D4	−2	2	−4	−6	0	4	−0.5	B	
E	6	E1	−4	−8	−6	2	4	−2	−3.5	1.0	
		E2	2	8	2	−6	−4	4	2.5	1.0	
		E3	−6	−4	−8	−4	2	2	−3.0	0.7	−
		E4	4	4	6	2	−2	0	2.5	N	
F	12	F1	−2	6	−2	−8	−4	4	1.0	0.2	−
		F2	4	−2	6	8	2	−4	1.0	0.8	−
		F3	2	8	4	−4	−6	2	3.0	1.0	
		F4	0	−6	−2	4	4	−2	−2.0	0.7	+
G	20	G1	−2	−2	−8	−4	4	6	−2.5	0.1	+
		G2	4	6	8	2	−4	−2	3.5	0.1	−
		G3	2	4	−4	−6	2	8	0.0	B	
		G4	0	−2	4	4	−2	−6	0.5	B	
H	−15	H1	4	8	6	−2	−4	2	3.5	0.5	+
		H2	−4	−8	−2	4	2	−6	−2.5	0.4	−
		H3	2	4	8	2	−6	−4	3.0	0.4	+
		H4	−2	−4	−6	0	4	2	−2.5	0.3	−
I	12	I1	−4	−6	2	4	−2	−8	−1.0	0.2	+
		I2	2	2	−6	−4	4	8	−1.0	0.0	
		I3	−6	−8	−4	2	2	−4	−3.0	0.8	+
		I4	4	6	2	−2	0	4	2.0	0.8	−
J	8	J1	−2	−8	−2	6	4	−4	−2.5	0.9	+
		J2	4	8	6	−2	−4	2	3.5	0.9	+
		J3	2	−4	4	8	2	−6	0.0	N	
		J4	0	4	−2	−6	−2	4	0.5	B	
K	−7	K1	4	6	8	2	−4	−2	3.5	0.5	+
		K2	−4	−2	−8	−6	2	4	−2.5	0.5	+
		K3	2	8	4	−4	−6	2	3.0	0.5	−
		K4	−2	−6	−4	2	4	0	−2.5	1.0	
L	15	L1	−4	2	−6	−8	−2	4	−1.0	B	
		L2	2	−6	2	8	4	−4	−1.0	B	
		L3	−6	−4	−8	−4	2	2	−3.0	0.2	+
		L4	4	2	6	4	0	−2	2.0	0.1	−

phase, these patterns should be related to each other with threefold rotation or mirror

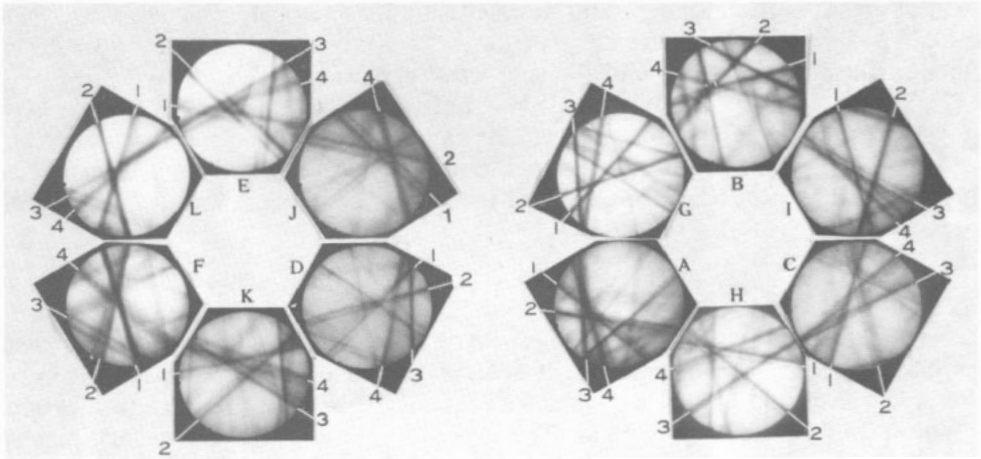

Figure 3. Experimental HOLZ line patterns along 12 equivalent zone axes.

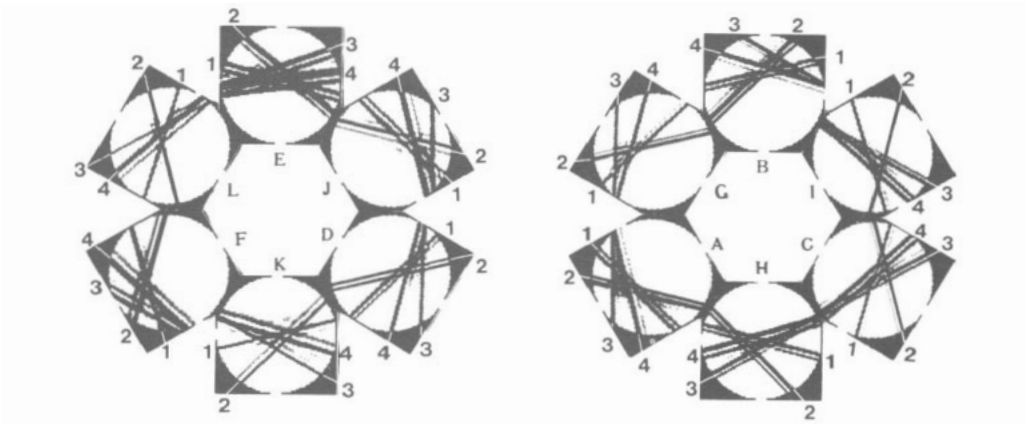

Figure 4. Simulated HOLZ line patterns along the 12 equivalent zone axes.

symmetry. However, they are quite different from each other in figure 3 because of the existence of the dislocation in the sample.

Figure 4 shows the corresponding simulated patterns. Comparing figure 4 with figure 3, we can see that they are in good agreement. The parameters used for the simulation are as follows: effective accelerating voltage, 100 kV; superlattice constant $a = 1.268$ nm, foil normal $\boldsymbol{F} \parallel [103]$; dislocation direction $\tilde{u} \parallel [\bar{2}\,1\,1\,2\,\bar{2}\,\bar{2}]$; Burgers vector $\bar{b} = 0.25[0\,1\,1\,0\,0\,0]$; thickness $t = 80$ nm; dislocation depth $d_d = 0.5t$. Here the value $0.5t$ of d_d implies that the electron probe is focused in the middle of the dislocation image for the experiments and that the point of the dislocation, which is closest to the calculation column, is at a depth of $0.5t$ for the simulation. In the present simulation, the dislocation is inclined to the specimen surface. Our previous work [4] shows that, when d_d/t varies around 0.5, the splitting behaviours of the HOLZ lines do not change very much. For the convenience of analysis and illustration we introduce two parameters.

(1) Normally a HOLZ line is split into two main lines, namely a strong fringe and another weak fringe. The intensity ratio of the weak fringe to the strong fringe is defined as the relative intensity of the split weak line, written as r.

(2) The position of the split weak line relative to the strong line is expressed as the sign of the difference between the deviation angles of the weak line and the strong line apart from Bragg condition written as sign(δ). When $\delta < 0$, it indicates that the weak line is at the positive side of the strong line along the projection of the reciprocal vector, and vice versa.

The last two columns in table 1 list the values of r and the signs of δ for the HOLZ reflections shown in figure 3. Equivalent effects to the splitting of HOLZ deficiency lines in the bright-field discs can be seen in the HOLZ rings. When several HOLZ lines intersect each other in the bright field, it is difficult to measure the intensity ratios solely from the bright-field disc. In this case, it is more accurate to measure the intensities from HOLZ reflections. The values of r listed in table 1 are the results obtained by combining the measurements of optical densitometry from the bright-field discs and the HOLZ reflections on negatives. The main points drawn from the experimental observations and the simulations are as follows.

(1) In patterns A and D, the HOLZ lines A3 and D3 do not appear to split, and lines C1, I1, I2, L1, L2, etc, show very weak splitting, i.e. their r values are approximately 0.0. All the traces of the planes corresponding to these HOLZ reflections intersect each other at poles near the [0 1 0] direction in figure 2. These imply that the values of $\bar{g} \cdot \bar{b}$ of the HOLZ reflections are very small and $b^{\parallel}$ is nearly parallel to the [0 1 0] direction. According to Zhang *et al* [2], $b^{\parallel}$ is parallel to one of the twofold axes. In the simulations, $\bar{b}$ equals 0.25[0 1 1 0 0 0] and this is true also in table 1. From table 1 we can see that the values of $\bar{g} \cdot \bar{b}$ of A3 and D3 equal zero and those of C1, L2, I1 and I2 are the smallest of the four main HOLZ lines in the corresponding pattern. (Generally, $g^{\perp}$ is much smaller than $g^{\parallel}$, so $g^{\perp} \cdot b^{\perp}$ is much smaller than $g^{\parallel} \cdot b^{\parallel}$ for a strong HOLZ reflection and $\bar{g} \cdot \bar{b} \simeq g^{\parallel} \cdot b^{\parallel}$.)

(2) In figure 3 the values of r and the signs of δ for the identical reflections I3 and B3, E3 and L3, and F3 and K3 are quite different from each other. The $\pm$ reflections D2 and G2, and J2 and A2 are also different apparently. According to Feng *et al* [4], the splitting of HOLZ lines may be affected by the foil thickness and the distance of the electron probe from the dislocation core. The distances d employed in the simulation are listed in table 2 where $d = -15$ nm and 12 nm for B and I, and $d = 15$ nm and 8 nm for A and J, respectively. The notation $d > 0$ indicates that the electron probe is focused on the side of the dislocation pointed to by $u \times z$ and vice versa, where z is the zone-axis direction. Additionally, the effective foil thickness is different for the different zone axes. In figure 4, the effective real thicknesses corresponding to J and A are about 81 nm and 98 nm, respectively, which result in the different separations between the split two fringes. This can also result in the different splitting feature for the $\pm$ reflections.

(3) In pattern L and the nearby patterns E, J, K and F, the separations between the two main fringes of the split HOLZ lines are rather wide. Computer simulations with the foil normal $F \parallel [1\,0\,3]$, which is close to the zone axis L, match the experimental patterns quite well. This shows that the large separations of split fringes are due to the small effective thickness.

(4) Pattern C in figure 3 is a weakly defocused pattern. The projection of the dislocation line can be drawn outwards from the centres of the distortional regions of

the HOLZ lines. It is seen that the HOLZ reflection C1 is parallel to the projectional line of the dislocation. To match the simulated HOLZ pattern with the experimental pattern, several different $\tilde{u}$ were used. The simulation with $\tilde{u} \parallel [\bar{2}\,1\,1\,2\,\bar{2}\,\bar{2}]$ matches the experimental pattern best. The projection of this direction is $[\bar{2}\,1\,0]$ which is close to the projection of C1, [10.2 3.1 0]. This indicates that the orientation $\tilde{u}$ of a dislocation, has an important influence on the splitting of the dislocation.

(5) By checking the values of r and signs of δ for each HOLZ line we can see that, in general, for the four HOLZ lines in each pattern, the larger the value of $\tilde{g} \cdot \tilde{b}$, the more severely the HOLZ line splits. The exceptions to this rule are E2, F2 and K4. On the other hand, we can see that the sign of $\tilde{g} \cdot \tilde{b}/d$ and the signs of δ for every HOLZ line in each pattern are opposite for the most markedly split HOLZ fringes except in the E, J and K patterns. Therefore we can divide the splitting behaviours of the HOLZ line patterns into two cases, namely the normal case and the anomalous case. In the normal case, the value of r and the sign of δ for each HOLZ line in a pattern approximately satisfy the following equations: $r \propto |\tilde{g} \cdot \tilde{b}/d|$, $\mathrm{sign}(\delta) = -\mathrm{sign}(\tilde{g} \cdot \tilde{b}/d)$. In the anomalous case, e.g. patterns K and E in figure 3, there is at least one HOLZ line for which the value of r or sign of δ does not satisfy the rules mentioned above. According to our simulation the anomalous case arises when the electron probe is too close to the dislocation, e.g. the dislocation-to-probe separation d is less than about 7 nm under the present conditions. Also, if d is larger than 30 nm, no obvious splitting of the HOLZ lines can be seen in the simulated pattern. However, it is difficult to determine the incident-probe-to-defect separation experimentally with good accuracy because the sizes of the contamination spots are much larger than that of the electron probe used and the probe may shift during operation. The values of d in table 1 are obtained mainly from simulation adjustments.

(6) From the good agreement between experiments and simulations, we believe that the dynamical theory for quasi-crystals developed by Cheng and Wang [3] is reliable.

5. Discussion

In the simulations, we did not consider the influence of the electron probe size on the CBED patterns. In fact the probe size in the experiments is about 4 nm. When the electron probe is very close to the dislocation, this influence becomes very strong and must be the important factor which causes the disagreement between the experimental pattern E in figure 3 and the corresponding simulation in figure 4. Additionally, the extraordinarily high intensities of F2 in figure 3 and figure 4 may result from the extraordinarily large value of $\tilde{g} \cdot \tilde{\epsilon}$ because, for F2, $\tilde{g} \cdot \tilde{b} = 1$ and $\tilde{g} \cdot \tilde{\epsilon} = 2.63$, which are the largest of the values for all the HOLZ reflections listed in table 1.

The splitting behaviours of the HOLZ lines in the quasi-crystalline icosahedral phase are quite similar to those of crystals [9, 10]. Nevertheless, owing to the special symmetry of the icosahedral phase, there are some new features in the splitting of the HOLZ lines of quasi-crystals. Studies of the whole strain field of a dislocation in a quasi-crystalline icosahedral phase by means of a defocus CBED pattern are in progress.

Acknowledgments

This project was supported by the National Natural Science Foundation of China.

References

[1] Wang R and Dai M 1990 *Phil. Mag. Lett.* **61** 119–23
[2] Zhang Z, Wollgarten M and Urban K 1990 *Phil. Mag. Lett.* **61** 125–31
[3] Cheng Y and Wang R 1989 *Phys. Status Solidi* b **152** 33–7
[4] Feng J, Zou H, Wang R, Yan Y and Dai M 1992 to be published
[5] Jones P M, Rackham G M and Steeds J M 1977 *Proc. R. Soc.* A **354** 197–222
[6] Hirsch P, Howie A, Nicholson R B, Pashley D W and Whelen M J 1977 *Electron Microscopy of Thin Crystals* (Huntington, NY: Robert E Krieger)
[7] Elser V 1985 *Phys. Rev.* B **32** 4892–8
[8] Zhao D, Wang R, Cheng Y and Wang Z 1988 *J. Phys. F: Met. Phys.* **18** 1893–904
[9] Tanaka M, Terauchi M and Kaneyama T 1991 *J. Electron Microsc.* **40** 211–20
[10] Zou H, Yao X and Wang R 1991 *Acta Crystallogr.* A **47** 490–7